Molecular modeling of EPON-862/graphite composites: Interfacial characteristics for multiple crosslink densities

C.M. Hadden[1], B.D. Jensen[1], A. Bandyopadhyay[1], G.M. Odegard[1]*, A. Koo[2], R. Liang[2],

[1]*Michigan Technological University, 1400 Townsend Drive, Houghton, MI 49931, USA*
[2]*High-Performance Materials Institute, Florida State University, Tallahassee, FL 32310, USA*

Abstract

Many thermo-mechanical properties of fiber-reinforced epoxy composites strongly depend on the conditions at the fiber/matrix interface. Because it is difficult to experimentally characterize the interface region, computational molecular modeling is a necessary tool for understanding the influence of interfacial molecular structure on bulk-level properties. The objective of this study is to determine the effect of crosslink density on the conditions of the interface region in graphite/epoxy composites. Molecular Dynamics models are developed for the fiber/matrix interfacial region of graphite/EPON 862 composites for a wide range of crosslink densities. The mass density, residual stresses, and molecular potential energy are determined in the epoxy polymer in the immediate vicinity of a graphite fiber. It is determined that a surface region exists in the epoxy in which the mass density is different than that of the bulk mass density. The effective surface thickness of the epoxy is about 10Å, irrespective of the crosslink density. A high-resolution TEM image is obtained for the interfacial region of carbon nanofiber/EPON 862 composites which clearly shows that the interface region thickness is about 10 Å, thus validating the molecular modeling technique. The simulations also predict residual stress levels in the surface region of the epoxy that are slightly higher than in the bulk, yet far below the ultimate load for the epoxy system considered herein. Furthermore, the simulations predict elevated levels of molecular potential energy in the interface region relative to the bulk epoxy, with the magnitude of energy decreasing for increasing crosslink densities.

KEYWORDS: A. Carbon fibres; B. Polymer-matrix composites (PMCs); B. Interface; B. Interphase; C. Modelling

1. Introduction

Graphite/epoxy composites are the prime components of many modern aircraft structures. These materials are lightweight and exhibit exceptional mechanical properties relative to their bulk mass density. The bulk-level mechanical properties of composites depend directly on the mechanical properties of the fiber and matrix and the physical and chemical conditions of the fiber/matrix interface. Strong adhesion between the fiber and matrix phases leads to improved load transfer from the matrix to the fibers which results in greater composite stiffness and strength, but lower toughness because of the absence of crack deflection mechanisms at the interface. In contrast, a weak fiber/matrix interface will provide lower composite strength with higher toughness [1, 2]. Because it is difficult to characterize the physical and chemical state of the fiber/matrix interface with experimental techniques, computational molecular simulation

techniques are necessary to design and develop tailored composite materials with desirable performance characteristics.

Many researchers have modeled pure thermosetting polymer systems using molecular dynamics (MD) techniques [3-6]. There has also been extensive research performed on the MD modeling of thermoset polymers containing nanotubes [7-11], nanofibers [12], and nanoparticles [13, 14]. Stevens [15] used a course-grained model to simulate interfacial fracture between a highly crosslinked polymer network and a solid surface. Mansfield and Theodorou [16] investigated the interface between graphite and a glassy polymer and determined that a 10 Å thick interfacial region existed in the polymer that was structurally different from that of the bulk polymer. Recently, Chunyu Li et al. [17] used MD simulations to observe the interface of a crosslinked thermoset polymer in the presence of a graphite surface. Although these studies have provided valuable information regarding the physical nature of the interfacial region in composites materials, they have not addressed the influence of crosslink density on the molecular structure of graphite/epoxy composite interfaces.

The purpose of this study was to determine the effect of crosslink density on the molecular structure of the fiber/matrix in a graphite/epoxy (EPON 862/DETDA) composite material. MD models were constructed for a wide range of crosslink densities and the molecular structure of the interface corresponding to each crosslink density was determined. The simulations predicted a polymer molecular structure at the interface that is different than that of the bulk polymer and is dependent on the crosslink density. The simulations were validated using TEM images of carbon nanofiber/epoxy composites that showed a similar molecular structure at the interface. The simulations were further used to predict the stresses and molecular potential energies in the interfacial region.

2. Molecular Modeling

This section describes the procedure for establishing the molecular model for the crosslinked epoxy/graphite interfaces. The procedure for establishing an equilibrated MD model of the uncrosslinked polymer/graphite interface is first detailed, followed by a description of the simulated crosslinking procedure. The LAMMPS (Large Scale Atomic/Molecular Massively Parallel Simulator) software package [18] was used for all of the Molecular Minimization(MM) and MD simulations described herein.

2.1 EPON 862-DETDA uncrosslinked structure

The initial uncrosslinked polymer molecular structure was established using a procedure similar to that of Bandyopadhyay et al. [3], consisting of the EPON 862 monomer and the DETDA hardener shown in Figure 1. A stoichiometric mixture of 2 molecules of EPON 862 and 1 molecule of DETDA was placed in a 10 x 10 x 10 Å MD simulation box with periodic boundary conditions. The initial atomic coordinates file was written in the native LAMMPS format and the OPLS (Optimized Potential for Liquid Simulations) United Atom force field developed by Jorgensen and co-workers [19, 20] was used for defining the bond, angle, and dihedral parameters. The OPLS United Atom force field calculates the total energy of the molecular

system by summing all of the individual energies derived from bond, angle, dihedral, and 12-6 Lennard-Jones interactions. The equilibrium spacing parameter σ of the Lennard-Jones potential was taken to be the arithmetic mean of the individual parameters of the respective atom types, while the well-depth parameter ε was taken to be the geometric mean of the values for the respective atom types. The non-bonded van der Waals interactions were modeled with an interaction cutoff radius of 10Å. This particular force field allows for modeling of CH_3, CH_2, CH, and alkyl groups as single united atoms with their corresponding masses. The described polymer model utilizes united atom structures for all applicable groups, except for the C and H atoms in the phenyl rings for both monomer and hardener molecules along with one CH_3 group directly connected to the phenyl ring of the DETDA molecule. Thus, the use of united atoms reduced the modeled 2:1 structure from 117 atoms to 83 atoms. The location of each united atom is shown in Figure 1, with 31 total atoms in the molecule of EPON 862 and 21 in the molecule of DETDA.
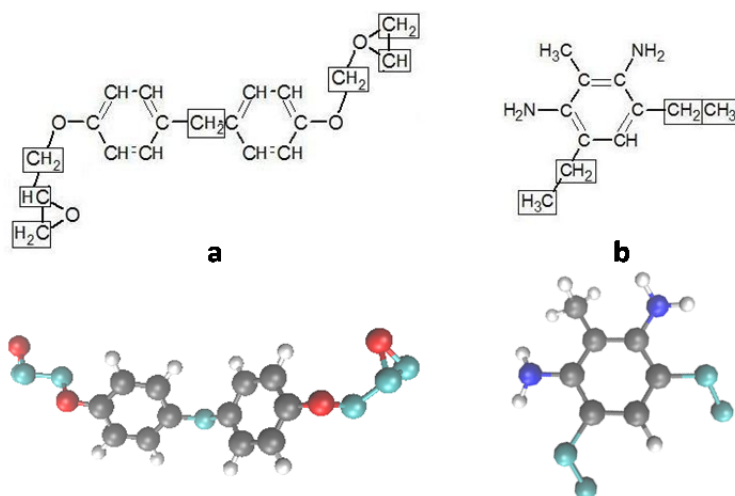

Figure 1. Molecular structures of a) EPON 862 and b) DETDA shown with simulated image. Top chemical structures show united atoms to be boxed, corresponding to the green beads in the simulated image.

The 2:1 molecular model was subjected to four MM minimizations and three MD simulations. This process minimized internal forces and thus reduced internal residual stresses which were created from the initial construction of bonds, bond angles, and bond dihedrals. After the structure stabilized to a relatively low energy value, the initial 2:1 stoichiometric structure was replicated, and the replicated models were randomly rotated and then translated along the x, y, and z axes and combined into a much larger structure containing 15,936 total united atoms. The resulting system consisted of many randomly oriented clusters of the small 2:1 ratio cluster stacked loosely together in a manner much like that of a simple cubic crystal structure. The newly created low-density structure had EPON 862:DETDA ratio of 394:192 with a box size of 64 x 66 x 115 Å. This larger model was then allowed to equilibrate into a uniform low-density liquid using a slow relaxation procedure performed over a cycle of 6 MM and 3 MD simulations. All MD simulations were conducted with the NVT (constant volume and temperature) ensemble for 100ps at 300K. A Nose/Hoover thermostat and barostat was implemented for temperature

and pressure control, respectively [21]. The initial box size produced a polymer density approximately equal to half of a fully cured solid EPON 862 epoxy (0.53 g/cc).
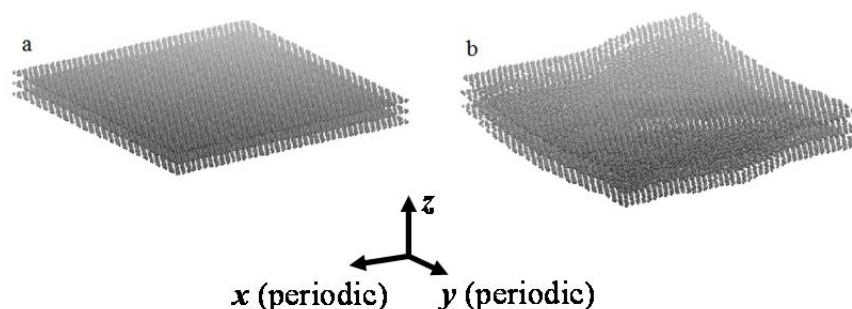

Figure. 2. a) Initial planar graphite structure and b) Graphite structure after equilibration

2.2 Graphite surface structure

The simulated graphite surface was constructed from 3 sheets of stacked graphene, each sheet containing 1,728 carbon atoms for a total of 5,184 atoms. The graphene sheets were oriented along the x-y plane, with periodic boundary conditions in the x and y-direction, and had an interlayer spacing of 3.35Å. Sheets were initially planar and contained no terminal hydrogens, surface imperfections, nor surface treatments. The graphite structures were relaxed using a series of MM and MD simulations, similar to that described above for the polymer structure. This initial equilibration step was performed without the presence of the polymer molecules. While equilibrating the graphite, the z-direction box coordinate was chosen to implement interlayer spacing for periodic boundary conditions. Thus the top surface was influenced by the bottom surface and visa-versa, representing many layers of bulk graphite. Initial and relaxed graphite structures are shown in Figure 2. Upon relaxation, the graphite structure was positioned to line up with the 64 x 66 Å dimension of the polymer structure.

2.3 Combining and condensing liquid polymer and graphite structures

It has been demonstrated that the molecular structure of a polymer matrix material near the interface of a reinforcing fiber is different than that in a pure bulk resin [16]. For this step in the procedure it was desired to simulate the non-crosslinked, low-density epoxy liquid resin in a parallelepiped simulation box surrounded on one side by the graphite structure, on the opposite side by the bulk epoxy resin, and on the remaining four sides by replicate images of the low-density liquid resin. This is shown on the left side of Figure 3 where the simulated polymer (labeled as "polymer") is situated above the graphite molecules along the z-axis and below a bulk polymer molecular structure. While the graphite and low-density polymer structures were established as described above, the bulk polymer structure is a fully crosslinked model of 76% crosslinked EPON 862/DETDA resin with a bulk density of 1.2 g/cc and 17,928 united atoms that was obtained previously [3]. Periodic boundary conditions were assumed along the x- and y-axes. Therefore, the molecular model effectively simulated an infinitely large, flat interface. Although fiber surfaces are round, the radius of curvature at the molecular level is large enough to effectively model it as a flat surface. An initial gap of 3.35 Å (interlayer spacing of graphite)

was placed between the graphite and polymer. The entire molecular model was equilibrated using two MM simulations and one 10 ps MD simulation. The entire model contained a total of 39,048 united atoms.
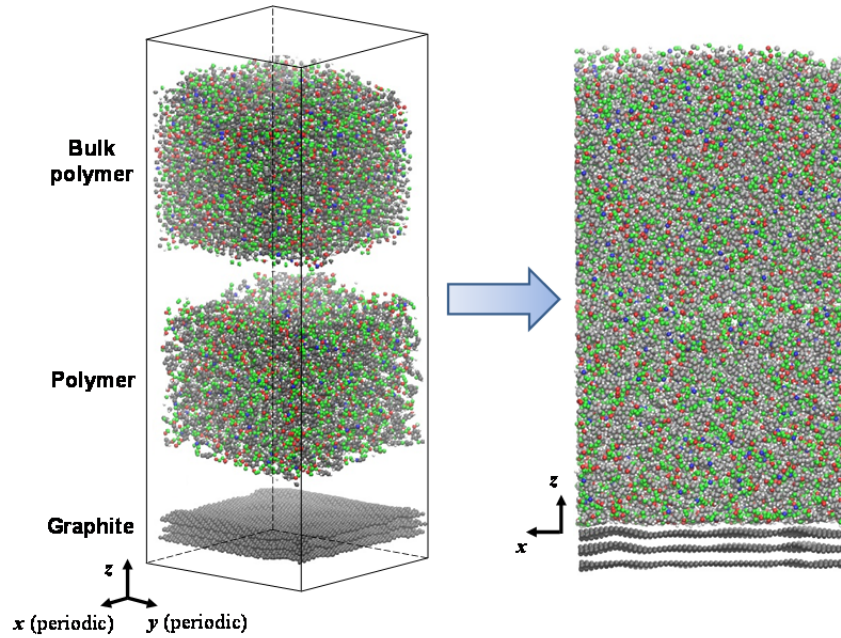

Figure 3. Combining three separate MD models (left) to form the complete MD model of the composite interface (right)

Following this initial equilibration step, the atoms of the bulk polymer and the graphite sheets were fixed and only non-bonded interactions between them and the polymer were considered for the remaining simulation processes. This step was performed to reduce computation time and to focus the simulations on the influence of the presence of the graphite sheet on the adjacent polymer molecular structure.

During the next step of establishing the composite interface molecular model, the simulated polymer molecules were condensed. The non-bonded van der Waals parameters were initially scaled down to prevent large increases in the energy of the system. In order to reach the appropriate polymer density, the atoms of the bulk polymer were displaced in small incremental amounts using the following equation,

$$z_i^{new} = z_i^{current} - S\left(z_i^{current} - z^{bottom}\right)$$

where z_i^{new} is the new z-coordinate for polymer atom i, $z_i^{current}$ is the current z-coordinate of polymer atom i, z^{bottom} is the lower-most polymer atom z-coordinate, and S is a scaling factor for the amount of displacement desired. For this study, S varied between 0.02 and 0.05, becoming smaller as the non-bonded van der Waals parameters were gradually scaled up again. Under this constraint, the polymer atom with the lowest z-coordinate value (nearest to the graphite) was not

displaced and the polymer atom with the highest z-coordinate (nearest to the bulk polymer) was displaced the most for each incremental step. The bulk polymer molecules were uniformly displaced the exact amount as the polymer atom with the highest z-coordinate, thereby continually condensing the polymer atoms. Each displacement was followed by a MM minimization and a 50ps MD simulation, followed lastly by another MM minimization. If a particular displacement step resulted in total energy values that were relatively high, the previous equilibration step was repeated before further condensation steps were taken. This process continued until achieving a polymer density of 1.16g/cc, totaling over 1 ns of MD simulation time. The resulting molecular model is shown on the right side of Figure 3.
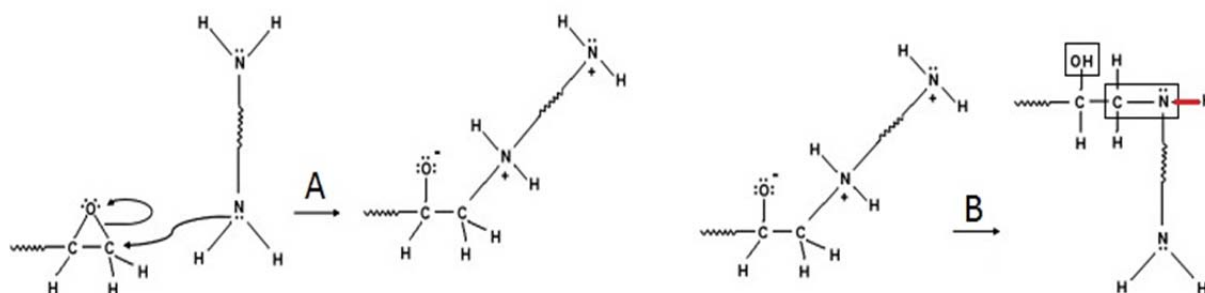

Figure 4. Crosslinking reaction: (A) Formation of primary C-N bond, leaving a negative charge on the oxygen and a positive charge on the nitrogen. (B) The negatively charged oxygen abstracts a proton from the neighboring amine, resulting in an alcohol group and an amine group. The reacted nitrogen is capable of forming another crosslink by the same reaction, breaking the N-H bond shown in red.

2.4 Crosslinking procedure

The equilibrated model was crosslinked based on the root mean square (RMS) distance between the CH_2 groups of the EPON 862 and the N atoms of DETDA molecules, similar to the method used by Yarovsky and Evans [22] and Bandyopadhyay et al. [3]. The modeled crosslinking reaction process is shown in Figure 4. Simultaneous breaking of the CH_2-O bonds in the epoxide ends of the EPON 862 molecules and N-H bonds of the DETDA molecules enable the activated CH_2 ends available to form crosslinks with activated N atoms of the DETDA molecules. A particular activated N can form a crosslink with the activated CH_2 for any adjacent EPON 862 molecule within a specified cut-off distance. Three assumptions were made for the crosslinking process:

1) Both primary amines in DETDA were assumed to have the same reactivity
2) The CH_2-O and N-H bonds were broken simultaneously (Figure 4 A)
3) The newly formed CH_2-N and O-H bonds were created simultaneously (Figure 4 B)

A flow chart describing the modeled crosslink reaction procedure is shown in Figure 5. After selecting an RMS cut-off distance, which affects the ultimate crosslink density of the MD model, and equilibrating the model; the RMS distances were determined between each pair of N atoms

and CH_2 united atoms within a specified cut-off distance. If multiple pairs (for a particular N or CH_2) were found within the cut-off, the closest pair was chosen for the crosslink reaction. Pairs outside the cut-off were not considered. The covalent bonds corresponding to these crosslink reactions were inserted into the MD model. The next step of the process was to identify and form the appropriate secondary bonds between the H atoms from the broken NH_2 groups and the O^- atoms of the epoxide ends. This bond was formed based on the closest RMS distances between the O^- and H^+ atoms. Because the newly formed bonds were capable of forming at distances greater than that of equilibrium, a multistep bond relaxation process was implemented (as shown in Figure 5) to avoid excessively high energies within the system. NVT simulations were implemented in the algorithm to achieve equilibration via pressure fluctuations. NPT simulations could not be used for this purpose because the necessary volume fluctuations were not compatible with the fixed positions of the carbon atoms in the graphene sheets.
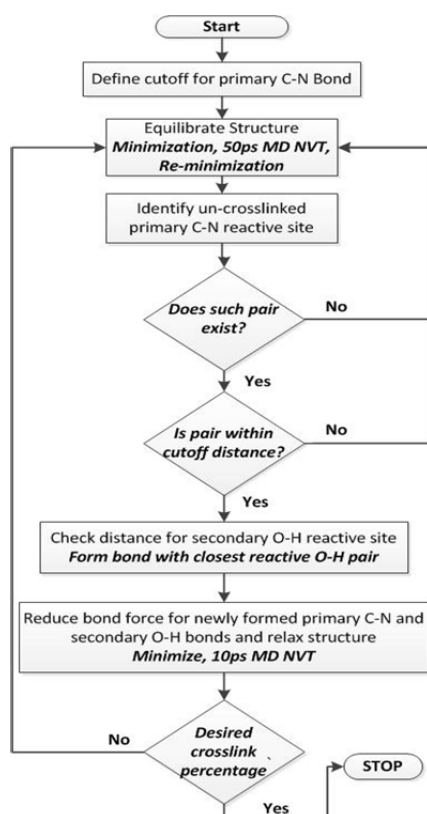

Figure 5. Flowchart describing crosslinking algorithm.

A total of six molecular systems were established, each having a unique crosslink density. The crosslink density was defined as the ratio of the total number of crosslinks that were formed to the maximum number of crosslinks that could be formed. For example, an epoxy network having 10 out of 20 crosslinks would have a crosslink density of 50%. The chosen crosslink densities were 57%, 65%, 70%, 75%, 80%, and 85%. The cut-off distances that were required to establish these specific crosslink densities ranged between 3.5 Å and 5 Å for the lowest and highest crosslink densities, respectively. These six unique systems were established using the procedure outlined in Figure 5 until the desired crosslink density was achieved. After crosslinking to the

desired density, each structure was allowed to equilibrate using 3 MM minimizations and 2 MD simulations of 1 nanosecond. The mass density of formed crosslink atoms (C-N and O-H) as a function of the z-axis can be seen in Figure 6, where the origin of the z-axis lies in the center of the top graphene sheet, as shown in Figure 3. It is important to note that the mass density of the crosslinks shown in Figure 6 are the mass densities associated with the crosslinking atoms. The figure shows good dispersion of crosslinks throughout the polymer structure with unique profiles for each crosslink density. Therefore, the crosslink distributions are relatively uniform and independent of crosslink density.
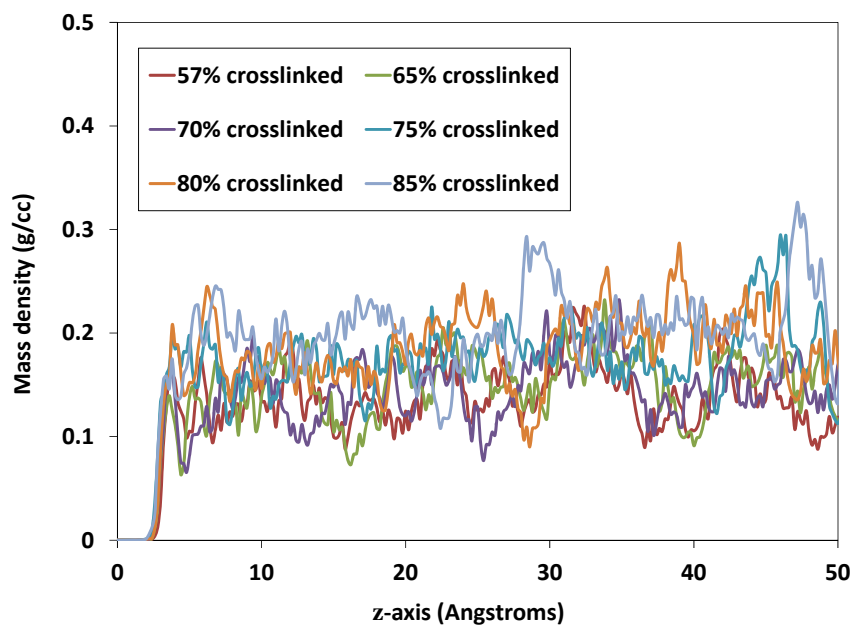

Figure 6. Crosslink atom mass density along z-axis for each crosslinked structure. Z-axis origin is taken from the center of mass of the closest graphene sheet.

3. Experimental validation

Because the predictions of the models need to be accurate and reliable, a sample of a carbon/epoxy composite was fabricated and analyzed using transmission electron microscopy (TEM) for model validation. The sample was established using a method discussed elsewhere [23] for an open-ended carbon nanofiber (PR-19-XT-HHT) reinforcing a crosslinked EPON 862/DETDA matrix. The image shown in Figure 7 was taken with a JEOL ARM20cF TEM and shows a portion of the open-ended nanofiber in the epoxy matrix. The cured bulk epoxy matrix is amorphous; however, a distinguishing band of structured interfacial phase can be seen on the surface of the nanofiber, as indicated in the figure. Although the thickness of this interface appears to vary in the image, the magnitude of the thickness is around 10 Å. This result will be discussed below in the context of model validation.
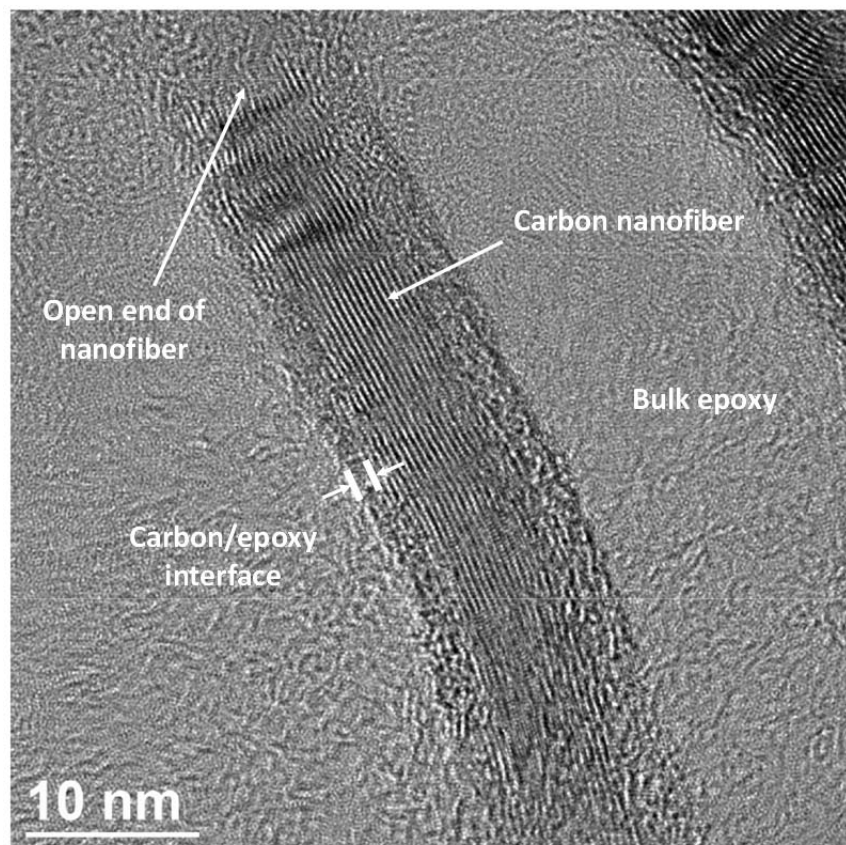
Figure 7. TEM image of a carbon nanofiber embedded in a crosslinked epoxy resin.

4. Results and Discussion

After the models were equilibrated, they were used to examine the effects of crosslink density on the overall polymer mass density at the polymer-graphite interface, the internal stress concentrations in the polymer at the interface, and the different potential energy components in the polymer. When examining some of the figures described below, it is important to note an important point regarding the calculation of mass densities on the molecular level. The traditional use of the term 'mass density' is on the continuum level, where the corresponding value reflects the local average mass of a continuous sample of volume and is usually a smooth, nearly constant value over the spatial domain of the volume. However, on the molecular level, the mass density is a strong function of spatial location in a molecular structure, and is thus not a constant value over the spatial domain. Therefore, the mass densities observed on the molecular level cannot be expected to match those on the continuum level.

4.1 Polymer Mass Density Characteristics

Mass densities were computed using the "fix/ave" spatial command in LAMMPS [18], which sums the per-atom densities and averages them for slices of a specified thickness along a specified axis. A slice thickness of 0.2 Å stacking along the z-axis was chosen to observe the structural change moving away from graphite surface oriented in the x-y plane. Figure 8 shows

the overall mass density profile for the three graphite sheets and polymer molecules at the interface. The finite width of the graphite sheet peaks is due to their slightly non-planar shape (Figure 2). The mass density of the polymer near the surface differs from that in the bulk with a profile similar to those reported for polymer systems with graphite [12, 18], carbon nanotube [10] and nanoparticle [13, 14] reinforcement. Common interfacial characteristics include (moving along the positive z-axis) an initial peak above bulk mass density, followed by a trough below bulk density, ending with a small peak above bulk density before leveling off.
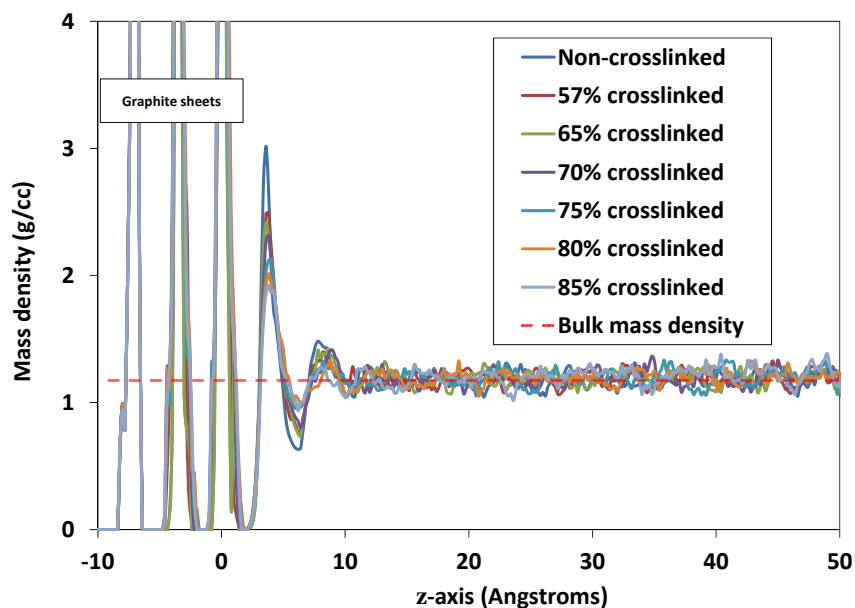

Figure 8. Mass density profile along z-axis of simulation box for graphite and polymer molecules. Z-axis zero value is taken as the center of the nearest graphite sheet. Polymer bulk density is shown by the red line (1.2 g/cc).

Figure 9 shows the same data shown in Figure 8, but focused on the interfacial region within 15 Å of the graphene sheet. The fluctuation in mass density is observed for about 10 Å from the center of the nearest graphite sheet. Therefore, the effective surface thickness of a polymer in the vicinity of graphite is about 10 Å. Figure 9 also demonstrates that the surface effects are reduced with increasing crosslink densities. As the polymer approaches higher crosslink densities, the mass density peak amplitudes reduce and the structure more closely resembles the bulk mass density distribution. This behavior is most likely due to the tendency of the crosslinks to hold the network together in a more spatially consistent manner.

The predictions shown in Figures 8 and 9 are supported by the atomic-resolution TEM image shown in Figure 7. Although the thickness of this interface shown in Figure 7 appears to vary in along the nanofiber length, the magnitude of the thickness is close to the predicted value, 10 Å. This favorable comparison verifies the existence of the molecular packing density variations predicted by the MD model and thus validates the modeling approach used herein.
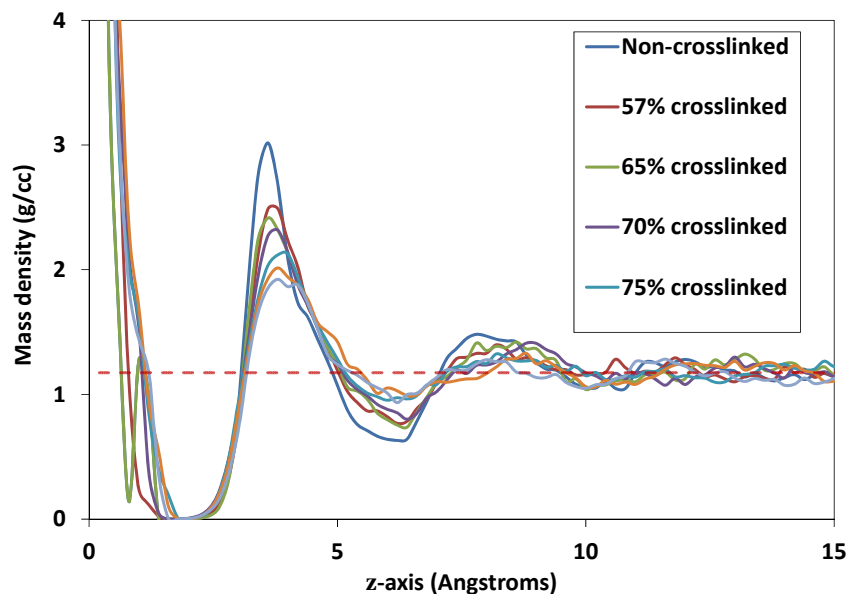
Figure 9. Interfacial mass density profile along z-axis of simulation box. Origin corresponds to center of nearest graphite sheet.
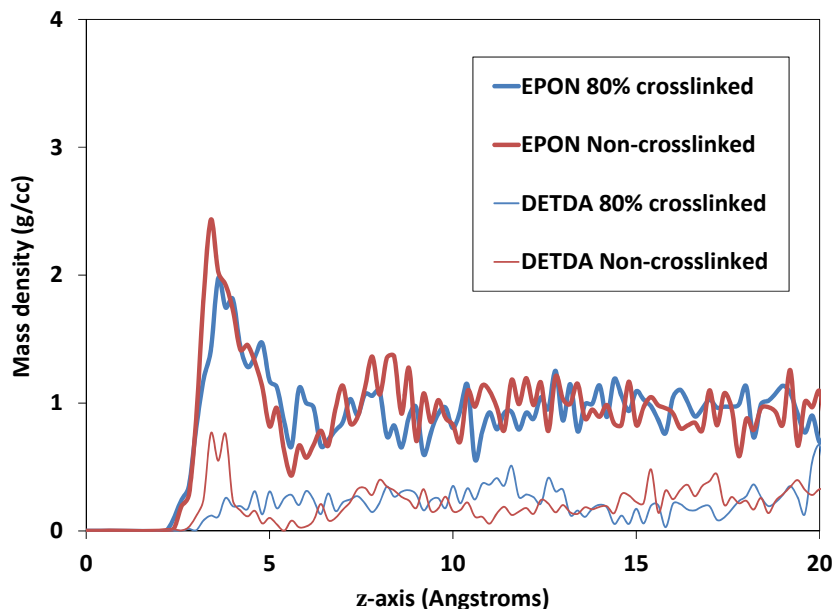

Figure 10. EPON and DETDA molecular mass densities along simulation box z-axis for Non-crosslinked and 80% crosslinked structures.

Figure 10 shows the mass density profiles for the EPON 862 and DETDA molecules for the non-crosslinked and 80% crosslinked systems. The mass densities were determined using the atoms associated with both molecules. That is, the atoms associated with the EPON and DETDA molecules were counted towards the EPON and DETA mass densities, respectively. In general, the data in Figure 10 demonstrate that densities of EPON 862 are larger than those of DETDA,

which is mostly because there are two EPON 862 molecules for every DETDA molecule. For both levels of crosslinking, larger concentrations of EPON are observed near the surface. Large concentrations of DETDA are only present at the surface for the non-crosslinked system. Therefore, before crosslinking occurs, both molecules are concentrated at the surface. During the process of crosslinking, the concentrated DETDA molecules are pulled away from the surface so that the DETDA mass density profile is relatively uniform.
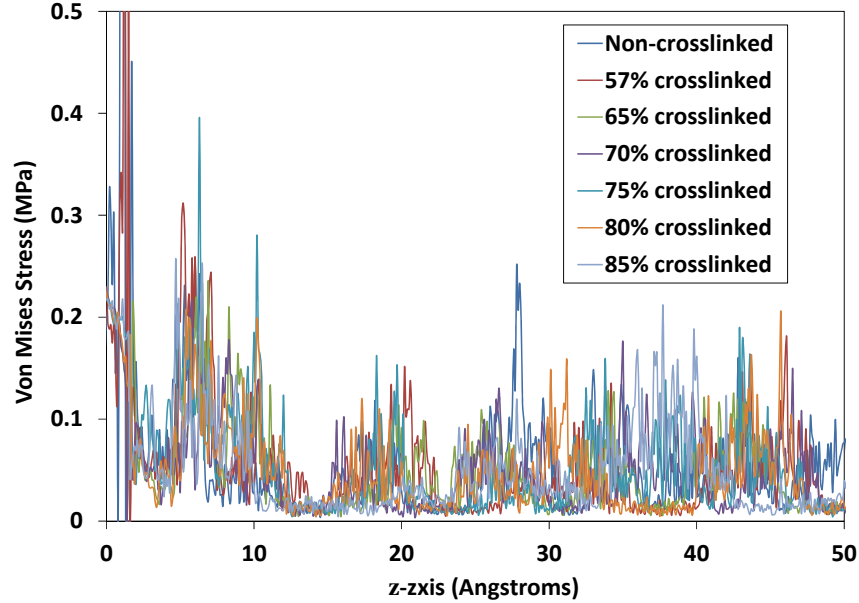

Figure 11. Spatially averaged Von Mises stress for polymer and graphite atoms along z-axis.

4.2 Polymer Internal Stress

Stress components were computed using the LAMMPS "fix/ave" spatial command in a similar manner as described above for the mass density profiles. Each normal and shear stress component was computed for each individual atom and averaged in slices of 0.1 Å along the z-axis of the simulation box. The individual stress components were then used to calculate the Von Mises stress using

$$\sigma_{VM} = \frac{1}{\sqrt{2}} \sqrt{\left(\sigma_x - \sigma_y\right)^2 + \left(\sigma_y - \sigma_z\right)^2 + \left(\sigma_z - \sigma_x\right)^2 + 6\left(\tau_{xy}^2 + \tau_{yz}^2 + \tau_{zx}^2\right)}$$

The Von Mises stress along the z-axis for a range of crosslink densities is shown in Figure 11. The stress peak nearest to the origin is due to stresses in the graphite sheet. Residual stresses are observed for each of the crosslink densities with the largest values at the interface. Despite the large amount of scatter in the data, there appears to be no influence of the crosslink density on the location and magnitude of residual stresses. The largest amount of stress in the polymer is considerably low for all crosslink densities, well below the expected tensile strength of EPON-862, which is 70-95 MPa at room temperature [24]. The presence of a small concentration of

residual stress near the interface indicates that upon significant loading of an epoxy/graphite composite, failure of the resin matrix would likely occur first near the fiber/matrix interface.
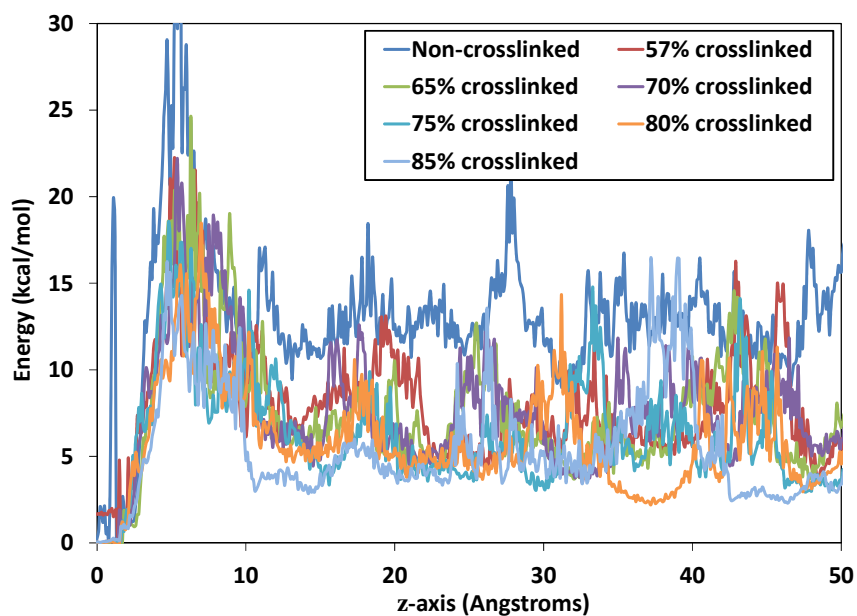

Figure 12. Spatially averaged per-atom potential energy. Potential energy values are the sum of bond, angle, dihedral, and non-bonded Van der Waals energies.

4.3 Polymer Potential Energy

Potential energy values for bonds, angles, dihedrals, and non-bonded interactions were computed with LAMMPS using the same fix/ave spatial command previously described. The bin size was 0.1 Å along the z-axis. Figure 12 shows the total potential energy (the sum of the individual energy terms) for each system. There appears to be an increased level of potential energy near the fiber/matrix interface, which is consistent with the increase in stress at the interface shown in Figure 11. Also, the potential energy generally decreases with increasing crosslink density. The largest contributing factor to the total potential energy was found to be angle energy, which decreases with increasing crosslink density. This is likely due to the elimination of the high-energy epoxide rings on the Epon 862 molecule during the crosslinking reaction. The decreases in potential energy with increasing crosslink density shown in Figure 12 indicate that crosslinking is energetically favorable for the modeled system and force field.

5. Conclusions

In this study, the influence of crosslink density on the molecular structure of the graphite fiber/epoxy matrix interface was examined using MD techniques. The modeled epoxy resin was an EPON 862/DETDA system. It was determined that the mass density of the polymer within 10 Å of the center of the nearest graphene sheet was perturbed from the bulk level of 1.2 g/cc. This observation agrees with predictions in the literature and our own TEM images. Although the amount of crosslink density did not influence this effective surface thickness of the epoxy near

the graphite interface, increasing levels of crosslinking reduced the magnitude of mass density fluctuations within the effective surface thickness. Analysis of the mass density of polymer molecules also reveals that before crosslinking, the presence of surface effects is due to both the perturbed mass densities of the EPON 862 monomer and DETDA hardener molecules in the surface region. Local Von Mises stresses were determined at the interface of the composite, and the MD simulations demonstrated that the internal stresses were slightly higher in the surface region than in the bulk epoxy, albeit at levels far below the ultimate strength of the neat resin. The internal stresses near the interface are not influenced by crosslink density. Finally, the MD simulations predict elevated levels of molecular potential energy in the surface region of the polymer, with the potential energy magnitude decreasing with increasing crosslink levels.

Acknowledgements

References

1.   Wagner, D.H. and R.A. Vaia, *Nanocomposites: Issues at the Interface.* Materials Today, 2004. 7(11): 38-42.
2.   Drzal, L.T. and M. Madhukar, *Fiber Matrix Adhesion and Its Relationship to Composite Mechanical-Properties.* Journal of Materials Science, 1993. 28(3): 569-610.
3.   Bandyopadhyay, A., P.K. Valavala, T.C. Clancy, K.E. Wise, and G.M. Odegard, *Molecular modeling of crosslinked epoxy polymers: The effect of crosslink density on thermomechanical properties.* Polymer, 2011. 52(11): 2445-2452.
4.   Varshney, V., S. Patnaik, A. Roy, and B. Farmer, *A Molecular Dynamics Study of Epoxy Based Networks: Cross-linking Procedure and Prediction of Molecular and Material Properties.* Macromolecules, 2008. 41(18): 6837-6842.
5.   Fan, H.B. and M.M.F. Yuen, *Material properties of the cross-linked epoxy resin compound predicted by molecular dynamics simulation.* Polymer, 2007. 48(7): 2174-2178.
6.   Li, C.Y. and A. Strachan, *Molecular dynamics predictions of thermal and mechanical properties of thermoset polymer EPON862/DETDA.* Polymer, 2011. 52(13): 2920-2928.
7.   Frankland, S.J.V., A. Caglar, D.W. Brenner, and M. Griebel, *Molecular Simulation of the Influence of Chemical Cross-Links on the Shear Strength of Carbon Nanotube-Polymer Interfaces.* Journal of Physical Chemistry B, 2002. 106(12): 3046-3048.
8.   Odegard, G.M., T.S. Gates, K.E. Wise, C. Park, and E.J. Siochi, *Constitutive modeling of nanotube-reinforced polymer composites.* Composites Science and Technology, 2003. 63(11): 1671-1687.
9.   Frankland, S.J.V., V.M. Harik, G.M. Odegard, D.W. Brenner, and T.S. Gates, *The Stress-Strain Behavior of Polymer-Nanotube Composites from Molecular Dynamics Simulation.* Composites Science and Technology, 2003. 63(11): 1655-1661.

10.   Clancy, T.C. and T.S. Gates, *Modeling of interfacial modification effects on thermal conductivity of carbon nanotube composites.* Polymer, 2006. 47(16): 5990-5996.
11.   Zhu, R., E. Pan, and A.K. Roy, *Molecular dynamics study of the stress-strain behavior of carbon-nanotube reinforced Epon 862 composites.* Materials Science and Engineering a-Structural Materials Properties Microstructure and Processing, 2007. 447(1-2): 51-57.
12.   Nouranian, S., C. Jang, T.E. Lacy, S.R. Gwaltney, H. Toghiani, and C.U. Pittman, *Molecular dynamics simulations of vinyl ester resin monomer interactions with a pristine vapor-grown carbon nanofiber and their implications for composite interphase formation.* Carbon, 2011. 49(10): 3219-3232.
13.   Odegard, G.M., T.C. Clancy, and T.S. Gates, *Modeling of the mechanical properties of nanoparticle/polymer composites.* Polymer, 2005. 46(2): 553-562.
14.   Yu, S., S. Yang, and M. Cho, *Multi-scale modeling of cross-linked epoxy nanocomposites.* Polymer, 2009. 50(3): 945-952.
15.   Stevens, M.J., *Interfacial Fracture between Highly Cross-Linked Polymer Networks and a Solid Surface: Effect of Interfacial Bond Density.* Macromolecules, 2001. 34: 2710-2718.
16.   Mansfield, K.F. and D.N. Theodorou, *Atomistic Simulation of a Glassy Polymer Graphite Interface.* Macromolecules, 1991. 24(15): 4295-4309.
17.   Li, C.Y., A.R. Browning, S. Christensen, and A. Strachan, *Atomistic simulations on multilayer graphene reinforced epoxy composites.* Composites Part a-Applied Science and Manufacturing, 2012. 43(8): 1293-1300.
18.   Plimpton, S., *Fast Parallel Algorithms for Short-Range Molecular-Dynamics* Journal of Computational Physics, 1995. 117(1): 1-19.
19.   Watkins, E.K. and W.L. Jorgensen, *Perfluoroalkanes: Conformational analysis and liquid-state properties from ab initio and Monte Carlo calculations.* Journal of Physical Chemistry A, 2001. 105(16): 4118-4125.
20.   Jorgensen, W.L., D.S. Maxwell, and J. Tirado-Rives, *Development and Testing of the OPLS All-Atom Force Field on Conformational Energetics and Properties of Organic Liquids.* Journal of the American Chemical Society, 1996. 117: 11225-11236.
21.   Hoover, W.G., *Canonical Dynamics - Equilibrium Phase-Space Distributions.* Physical Review A, 1985. 31(3): 1695-1697.
22.   Yarovsky, I. and E. Evans, *Computer simulation of structure and properties of crosslinked polymers: application to epoxy resins.* Polymer, 2002. 43(3): 963-969.
23.   Koo, A.C., Y.F. Su, J.G. Park, R. Liang, B. Wang, and C. Zhang. *Interactions of Resin Matrix and Open ends of Carbon Nanotubes and Carbon Nanofibers in Composites*. in *International SAMPE Technical Confernence*. 2011. Fort Worth, TX.
24.   Littell, J.D., C.R. Ruggeri, R.K. Goldberg, G.D. Roberts, W.A. Arnold, and W.K. Binienda, *Measurement of epoxy resin tension, compression, and shear stress-strain curves over a wide range of strain rates using small test specimens.* Journal of Aerospace Engineering, 2008. 21(3): 162-173.